RESEARCH PAPER

Development and Optimization of Doxorubicin-Loaded Modified Chitosan Nanoparticles: A Quality by Design Approach for Enhanced Anticancer Efficacy

Sushama hari Garud*1| Rahul Laxman Jadhav2| Vyaknatesh Ravindra Dharanguttikar3

ABSTRACT

Background: Chitosan-based nanocarrier has emerged as promising drug delivery systems for cancer chemotherapy; however, their clinical translation remains limited by suboptimal drug loading, premature release, and inconsistent physicochemical properties. Chemical modification of chitosan offers opportunities to overcome these limitations through enhanced mucoadhesion, sustained release, and improved targeting capabilities.

Aim: This study aimed to synthesize and characterize a novel modified chitosan derivative and develop doxorubicin-loaded nanoparticles using a logical Quality by Design (QbD) approach to ensure robust, reproducible formulations with superior anticancer activity.

Method: Modified chitosan was synthesized and comprehensively characterized using elemental analysis, ^{1}H NMR, FT-IR spectroscopy, and mass spectrometry. Doxorubicin-loaded nanoparticles were prepared via the ionic gelation technique and optimized using a QbD approach. The optimized formulation was further characterized for particle size, zeta potential, X-ray diffraction (XRD), scanning and transmission electron microscopy (SEM/TEM), differential scanning calorimetry (DSC), and in vitro drug release. Anticancer activity was assessed using MTT, SRB, and XTT cytotoxicity assays, while apoptotic potential was evaluated through the trypan blue exclusion assay.

Result: Spectroscopic and analytical studies confirmed successful chemical modification of chitosan while preserving its essential functional groups. The QbD-optimized formulation (F1) exhibited favorable physicochemical characteristics, including a zeta potential of −25.3 mV, particle size of 223.4 nm, PDI of 0.019, encapsulation efficiency of 88.04%, and drug loading of 7.52%. Solid-state analyses indicated molecular dispersion of doxorubicin within the polymer matrix, confirming efficient encapsulation. The optimized nanoparticles showed pH-responsive sustained drug release (29.73% at pH 7.4 and 46.51% at pH 5.5 over 12 h) and significantly enhanced cytotoxicity in multiple cell viability assays (IC_{50} = 70.69 µg/mL in the MTT assay), along with pronounced apoptotic induction compared to free doxorubicin, suggesting improved cellular uptake and therapeutic efficacy.

Conclusion: The modified chitosan-based nanoparticulate system developed through systematic QbD principles represents a promising platform for enhanced doxorubicin delivery with superior anticancer activity. This approach demonstrates the value of polymer modification combined with rational formulation design in advancing nanomedicine for cancer therapy.

Keywords: Modified Chitosan, Doxorubicin, Nanoparticles, Quality by Design, Ionic Gelation, Anticancer Activity, Apoptosis.

How to cite this article: Garud SH, Jadhav RL, Dharanguttikar VR. Development and Optimization of Doxorubicin-Loaded Modified Chitosan Nanoparticles: A Quality by Design Approach for Enhanced Anticancer Efficacy. Int J Drug Deliv Technol. 2026;16(14s): 154-174. DOI: 10.25258/ijddt.16.14s.22

Introduction

Considering an expected 10 million deaths worldwide in 2024 and a major strain on healthcare systems worldwide, cancer continues to be one of the most difficult problems in modern medicine.[1] Conventional chemotherapy remains a key component of cancer treatment regimens, despite notable advancements in our knowledge of cancer biology and the creation of targeted medicines. However, systemic toxicity, nonspecific biodistribution, poor pharmacokinetic profiles, and the emergence of multidrug resistance significantly limit the clinical value of many powerful anticancer drugs.[2] An example of these difficulties is the anthracycline antibiotic doxorubicin (DOX). Despite being acknowledged as one of the most potent chemotherapeutic agents against a wide range of cancers, such as solid tumors, lymphomas, and breast cancer, dose-dependent cardiotoxicity, myelosuppression, and the development of drug resistance mechanisms restrict its clinical use. Free doxorubicin accumulates significantly in healthy tissues, especially the myocardium, due to its nonselective distribution, which causes congestive heart failure and permanent cardiomyopathy.[3] These restrictions have spurred extensive

research on nanocarrier-based delivery systems that can increase tumor accumulation through the increased permeability and retention (EPR) effect while reducing systemic exposure, hence improving the therapeutic index of doxorubicin. Chitosan-based nanoparticles have attracted a lot of interest among the different nanocarrier platforms being studied for anticancer drug delivery because of its innate biocompatibility, biodegradability, mucoadhesive qualities, and positive surface charge that promotes cellular contact.[4] The linear polysaccharide chitosan, which is produced by partially deacetylating chitin, has special physicochemical characteristics, such as pH-responsive behavior and reactive hydroxyl and amino groups that can be chemically altered. Nevertheless, native chitosan has some drawbacks, including as pH-dependent solubility, comparatively poor mechanical qualities, and quick dissolving at physiological pH, which might lead to early drug release and less-than-ideal pharmacokinetic profiles.[5] Chemical modification of chitosan via conjugation, crosslinking, or grafting with different functional moieties has become a tactical method to get around these intrinsic restrictions. New functional groups that improve drug-polymer interactions, increase stability at physiological pH, alter degradation rates, and add stimuli-responsive properties can all be introduced by such alterations.[6] According to recent research, modified chitosan derivatives outperform unmodified chitosan in terms of drug loading capacity, controlled release behavior, and biological activity. Additionally, by increasing cellular absorption pathways or introducing targeted ligands, these alterations can improve treatment effects.[7] Despite these encouraging advancements, batch-to-batch variability, reproducibility problems, and a lack of knowledge on formulation-performance linkages have made it difficult to move chitosan-based nanoformulations from the bench to the bedside.[8] Conventional formulation development methods focused on one-factor-at-a-time (OFAT) optimization frequently produce unsatisfactory products with unexpected quality attributes because they are unable to capture complicated interactions between formulation factors.[9] Endorsed by regulatory bodies such as the FDA and EMA, the QbD (Quality by Design) paradigm provides a methodical, scientific method for developing pharmaceuticals that prioritizes risk assessment, design space establishment for robust manufacturing, and comprehension of product and process variables.[10] The Quality Target Product Profile (QTPP), which describes the intended quality attributes of the finished product based on therapeutic aims, is the first step in the QbD technique. Critical Material Attributes (CMAs) and Critical Process Parameters (CPPs) that affect CQAs are then evaluated, and Critical Quality Attributes (CQAs)—parameters that directly affect product performance and safety—are identified.[11] The relationship between input variables and CQAs can be quantitatively determined by risk assessment techniques like Effect Analysis (FMEA), Failure Mode and systematic experimentation using DoE (Design of Experiments), allowing optimization within a specified design area. By showcasing process comprehension and control plan, this method not only improves product quality and process efficiency but also makes regulatory approval easier. A logical approach to creating improved nanocarrier systems with consistent, repeatable performance characteristics is to combine chitosan modification with QbD-driven formulation development.[12] Nevertheless, there are still few extensive investigations in the literature that integrate these methods with careful structural characterisation of modified polymers and exacting assessment of anticancer activity. Additionally, the majority of studies assess cytotoxicity using a single assay, which may not give a comprehensive picture of anticancer mechanisms, especially the crucial distinction between cytotoxic and cytostatic effects.[13] Therefore, the current study were designed with the following goals in mind: (1) to synthesize and thoroughly characterize a novel modified chitosan derivative using multiple analytical techniques to confirm structural modification; (2) to develop doxorubicin-loaded nanoparticles using ionic gelation technique with systematic application of QbD principles for formulation optimization; (3) to perform extensive physicochemical and solid-state characterization of the optimized formulation to establish structure-property relationships; and (4) to evaluate the anticancer efficacy of the nanoformulation using multiple complementary cytotoxicity assays and apoptotic index determination to fully assess therapeutic potential.[14] In order to create a clinically transferable nanoformulation, this work takes a comprehensive approach that integrates polymer chemistry, formulation science, quality risk management, and pharmacological evaluation. The methodical approach used here offers a path forward for the logical creation of polymer-based nanocarrier systems with improved therapeutic efficacy and regulatory acceptance.[15]

Materials

We purchased chitosan from Sigma-Aldrich (Mumbai) with a medium a degree of deacetylation of 75–85% and molecular weight. We purchased pharmaceutical-grade, ≥98% pure doxorubicin hydrochloride from TCI Chemicals (Mumbai). We bought analytical-grade sodium tripolyphosphate (TPP) from Merck KGaA (Mumbai). Every chemical reagent used to modify chitosan was of analytical or reagent quality and was purchased from reputable commercial vendors. Cambridge Isotope Laboratories (Pune) supplied the deuterated solvents (D_2O, DMSO-d_4, and DCl) for NMR spectroscopy. Gibco/Thermo Fisher Scientific (Mumbai) provided the cell culture media (DMEM, RPMI-1640), fetal bovine serum (FBS), phosphate-buffered saline (PBS, pH 7.4), and penicillin-streptomycin solution. Sigma-Aldrich supplied MTT (3-(4,5-dimethylthiazol-2-yl)-2,5-diphenyltetrazolium bromide), SRB (sulforhodamine B), XTT (2,3-bis-(2-methoxy-4-nitro-5-sulfophenyl)-2H-tetrazolium-5-carboxanilide), and trypan blue dye. The American Type Culture Collection (Mumbai) provided the cancer cell lines. The remaining chemicals and reagents were analytical grade and were utilized without additional purification. Throughout the investigation, ultrapure water (resistivity 18.2 MΩ·cm) from a Milli-Q system was utilized.

METHODS

Synthesis of Modified Chitosan

In a clean, dry conical flask, 0.5 g of chitosan was dissolved in 50 mL of pyridine under continuous stirring. Subsequently, 4 mL of chloroacetyl chloride was added gradually with constant swirling. The reaction mixture was allowed to stand for 24 h to ensure complete reaction. The resulting solid product was filtered and thoroughly washed with ethanol to remove residual solvent and unreacted reagents, then dried and its melting point was determined. The dried product was dispersed in 20 mL of ethanol, followed by the addition of 0.5 mL of ammonia solution, and stirred for 2 h. Finally, the mixture was filtered, washed with ethanol, and dried to obtain the modified chitosan derivative for further characterization and evaluation.[16]

Characterization of Modified Chitosan

Elemental Analysis

A CHN/S elemental analyser (STIC, Cochin University of science and technology campus, Kochi) were used to determine the elemental composition (carbon, hydrogen, nitrogen, and sulfur) of both native and modified chitosan. Samples were carefully weighed (3–5 mg) into tin capsules and burned in excess oxygen at a high temperature. Gas chromatography was used to separate the resultant combustion gases, and thermal conductivity detection was used to quantify them. Using established mathematical connections, the degree of substitution (DS) was computed based on the change in nitrogen content prior to and following alteration.

Fourier Transform Infrared (FT-IR) Spectroscopy

An FT-IR spectrophotometer (Nicolet iS50, Thermo Fisher Scientific, USA) fitted with an attenuated total reflectance (ATR) accessory was used to record the FT-IR spectra of native chitosan, modified chitosan, and pertinent starting materials. In the wavenumber range of 4000-400 cm^{-1}, samples were directly examined without preprocessing using 32 scans per sample and a resolution of 4 cm^{-1}. Prior to every sample measurement, background spectra were gathered. OMNIC software was used to process the spectral data, and distinctive peaks were found and compared to verify the addition of new functional groups that would indicate a successful change.

Nuclear Magnetic Resonance (NMR) Spectroscopy

A high-resolution NMR spectrometer (AVANCE III HD 400 MHz, Bruker BioSpin, Switzerland) was used to obtain ^1H and ^{13}C NMR spectra at room temperature. To achieve full dissolution, materials were dissolved in D_2O with a little amount of DCl for ^1H NMR analysis. Broadband proton decoupling was used to acquire ^{13}C NMR spectra at 100 MHz. Chemical shifts (δ) were expressed in parts per million (ppm) and compared to either the residual solvent peak or an internal standard (3-(trimethylsilyl)propionic-2,2,3,3-d_4 acid sodium salt, TSP). The unit of measurement for coupling constants (J) was hertz (Hz). TopSpin software (Bruker) was used to process and evaluate the spectra, and when required, two-dimensional NMR experiments (COSY, HSQC) and comparison with literature values were used to assign peaks.

Mass Spectrometry

Electrospray ionization (ESI) in conjunction with a mass spectrometer (Q-TOF LC/MS, Agilent Technologies, USA) was used for mass spectrometric analysis. Samples were infused straight into the ion source after being dissolved in the proper solvents (usually methanol or water with formic acid). To get complete molecular information, both positive and negative ionization modalities were assessed. Data were collected across a suitable m/z range while the mass spectrometer was running with optimum source parameters. The molecular formula and degree of modification were confirmed by comparing observed and theoretical isotopic patterns.[17]

Quality by Design (QbD) Approach for Formulation Development

Quality Target Product Profile (QTPP)

The therapeutic goals, expected mode of administration, and intended product attributes were taken into consideration when defining the QTPP. Dosage form (nanoparticulate suspension for intravenous administration), particle size (100-300 nm to maximize EPR effect and prevent rapid clearance), zeta potential (positive, >+20 mV for colloidal stability and enhanced cellular interaction), drug loading (enough to achieve therapeutic dose in a reasonable injection volume), encapsulation efficiency (>70% to ensure economic viability), drug release profile (sustained release over 24-48 hours to maintain therapeutic drug levels), and physicochemical stability (maintenance of critical attributes over the intended shelf life).[18]

Identification of Critical Quality Attributes (CQAs)

The following CQAs were shown to directly affect product safety and efficacy based on the QTPP and existing knowledge: Zeta potential controls colloidal stability and cellular interaction; encapsulation efficiency and drug loading determine therapeutic payload and dose requirements; particle size and polydispersity index (PDI) affect biodistribution, tumor penetration, and clearance kinetics; and in vitro drug release rate reflects in-vivo pharmacokinetic behaviour.[19]

Risk Assessment: Identification of Critical Material Attributes (CMAs) and Critical Process Parameters (CPPs)

Ishikawa (fishbone) diagrams, Effect Analysis (FMEA) and Failure Mode were used in a methodical risk assessment to material characteristics and process parameters that influence effect of CQAs.

Critical Material Attributes (CMAs)

Altered chitosan concentration in the formulation, which controls particle formation and size; altered chitosan molecular weight and degree of substitution, which impact polymer chain interactions and drug encapsulation; TPP concentration, which affects particle properties and crosslinking density; pH of the modified chitosan solution, which affects polymer solubility and ionic interactions; and doxorubicin concentration, which affects drug loading and encapsulation efficiency.

Critical Process Parameters (CPPs)

Temperature during preparation, which affects polymer behaviour and ionic interactions; stirring time, which affects particle maturation and size stabilization; TPP addition rate, which affects the kinetics of ionic gelation and particle uniformity; and modified chitosan to TPP ratio, which determines crosslinking extent and particle properties. High-risk factors were given priority for experimental inquiry based on risk priority numbers (RPN), which were computed as the product of severity, occurrence, and detectability scores.[19]

Design of Experiments (DoE) and Optimization

To determine ideal formulation conditions and assess the impact of essential components on CQAs, a methodical experimental methodology was utilized. Depending on how many aspects needed to be examined, a Box-Behnken or central composite design was used. zeta potential, Particle size, PDI and encapsulation efficiency were the dependent factors (responses), whereas modified chitosan concentration, TPP concentration, and stirring speed were the independent variables. Design-Expert software (Stat-Ease Inc., Minneapolis, MN, USA) or JMP software (SAS Institute, USA) were used for statistical analysis. Polynomial models connecting independent factors to responses were created using response surface methodology (RSM). Coefficient of determination (R2), analysis of variance (ANOVA), adjusted R2, predicted R2, and lack of fit tests were used to evaluate the model's adequacy. The link between variables and responses was visualized using three-dimensional response surface plots and contour plots. The best formulation that concurrently satisfied all predetermined criteria for CQAs was found by numerical optimization utilizing the desirability function approach. The design space was created and displayed to reflect the multidimensional combination and interplay of input variables that have been shown to guarantee quality.[20]

Preparation of Doxorubicin-Loaded Modified Chitosan Nanoparticles

An ionic gelation method refined with a Quality by Design (QbD) methodology was used to create doxorubicin-loaded nanoparticles. To promote drug–polymer interaction, an aqueous solution of doxorubicin hydrochloride was added after modified chitosan was dissolved in diluted acetic acid (pH = 5.0) while being continuously stirred. Instantaneous ionic crosslinking between protonated chitosan amino groups and TPP phosphate moieties was caused by the dropwise addition of sodium tripolyphosphate (TPP) solution at the optimal concentration under carefully regulated stirring conditions, which started the creation of nanoparticles. To guarantee particle stability, the dispersion was further agitated. The resultant nanoparticles were gathered,

lyophilized using trehalose as a cryoprotectant, then centrifuged to remove any remaining chemicals and unentrapped drug. Before being further characterized and assessed, the dried nanoparticles were kept at -20 °C.[21]

Physicochemical Characterization of Nanoparticles

Particle Size, Polydispersity Index (PDI), and Zeta Potential

Using a Zetasizer Nano ZS (Malvern Panalytical, UK), dynamic light scattering (DLS) and electrophoretic light scattering (ELS) were used to assess the particle size distribution, zeta potential, and PDI. To prevent multiple scattering effects, nanoparticle suspensions were suitably diluted with ultrapure water. Samples were equilibrated at 25°C for size measurements, and the intensity distribution was used to calculate the z-average diameter and PDI. Samples were put in disposable folded capillary cells for zeta potential measurements. The Smoluchowski equation was used to translate electrophoretic mobility to zeta potential. Every measurement was done in triplicate, and the mean ± standard deviation was used to express the results.

Encapsulation Efficiency and Drug Loading

An indirect method were used to calculate drug loading (DL %) and encapsulation efficiency (EE %). After centrifuging the nanoparticle suspension at a high speed, the unentrapped drug-containing supernatant was carefully recovered. After creating a calibration curve with known doxorubicin concentrations, the amount of free doxorubicin in the supernatant were measured by spectrophotometrically at 480 nm using a UV-visible spectrophotometer (Marc, Mumbai). The following formulas were used to determine EE% and DL%:

Encapsulation Efficiency (EE %) = [(Total drug - Free drug) / Total drug] × 100 Drug Loading (DL %) = [(Total drug - Free drug) / Weight of nanoparticles] × 100

Differential Scanning Calorimetry (DSC):

The physical state of doxorubicin in the nanoparticles and any drug-polymer interactions were examined through thermal analysis using a differential scanning calorimeter (DSC 25, TA Instruments, USA). Sealed aluminum pans were filled with precisely weighed samples (3–5 mg) of pure doxorubicin, native chitosan, modified chitosan, a physical combination of drug and polymer, blank nanoparticles, and drug-loaded nanoparticles. The reference was an empty, sealed pan. Samples were heated under nitrogen purge over a suitable temperature range at a steady rate of 10°C/min. TRIOS software (TA Instruments) was used to record and analyze DSC thermograms. Melting, glass transition, and breakdown are examples of typical thermal phenomena that were found and compared amongst samples.

X-ray Diffraction (XRD)

An X-ray diffractometer (D8 Advance, Bruker AXS, Germany) with Cu Kα radiation (λ = 1.5406 Å) was used to obtain X-ray diffraction patterns. Samples were scanned over a 2θ range of 5° to 50° with a step size of 0.02° and a scanning rate of 2°/min on low-background silicon holders. The operating current and voltage were set at 40 kV and 40 mA, respectively. To evaluate the drug's crystallinity and identify any possible production of amorphous drug or molecular dispersion inside the polymer matrix, XRD patterns of pure doxorubicin, modified chitosan, physical mixture, and drug-loaded nanoparticles were evaluated.[22]

3.5.5. Scanning Electron Microscopy (SEM)

A field emission scanning electron microscope (FESEM, JSM-7600F) was used to analyse the surface morphology of the lyophilized nanoparticles. To improve electrical conductivity, samples were sputter-coated with a thin coating of gold-palladium (about 5 nm) using a sputter coater after being mounted on aluminum stubs using double-sided carbon adhesive tape. An accelerating voltage of 5–10 kV was used to take pictures at different magnifications. The micrographs were used to evaluate the size distribution, surface texture, and particle shape.

Transmission Electron Microscopy (TEM) Transmission electron microscopy (TEM, JEM-2100, JEOL) was used to analyze the nanoparticles' precise particle size and internal structure. On a carbon-coated copper grid, a drop of suitably diluted nanoparticle suspension was deposited and either left to dry at room temperature or negatively stained with uranyl acetate solution or phosphotungstic acid for increased contrast. A CCD camera was used to take digital pictures while the grids were inspected at an accelerating voltage of 120–200 kV. Using ImageJ software (NIH, Bethesda, MD, USA), at least 100 particles were measured in order to estimate the particle size distribution.[23]

***In-Vitro* Drug Release Studies**

To assess the release behaviour of doxorubicin from the nanoparticles under physiological and tumor-mimicking settings, in vitro drug release tests was carried out by utilizing the dialysis bag diffusion method. Phosphate-buffered saline (pH 7.4) or acetate buffer (pH 5.5) were used to submerge dialysis membranes (MWCO 12–14 kDa) containing a specific quantity of drug-loaded nanoparticles. The membranes were then incubated in a shaking water bath at 37 ± 0.5 °C and 100 rpm. To sustain sink settings, aliquots

of the release medium were removed and exchanged with new buffer at prearranged intervals up to 72 hours. The cumulative drug release was plotted as a purpose of time after the released doxorubicin was measured spectrophotometrically at 480 nm. For comparison, release from free doxorubicin solution was assessed under the same circumstances. Using DDSolver software, the release data were fitted to zero-order, first-order, Higuchi, Korsmeyer–Peppas, and Hixson–Crowell kinetic models in order to clarify the release process. Based on the and lowest Akaike Information Criterion (AIC) and highest coefficient of determination (R^2), the best-fitting model was chosen. The dominating release mechanisms were described by using the release exponent (n) derived from the Korsmeyer–Peppas model.[24]

***In-Vitro* Anticancer Activity Evaluation:**

Cell Culture Human cancer cell lines that are pertinent to doxorubicin treatment, such as MCF-7 breast adenocarcinoma, HepG2 hepatocellular carcinoma, or A549 lung carcinoma cells, were grown in the proper culture medium (DMEM or RPMI-1640) supplemented with 1% penicillin-streptomycin solution and 10% fetal bovine serum. The cell was kept at 37°C and 5% CO2 in a humidified incubator. Cells were subcultured using trypsin-EDTA solution after they reached around 80% confluence, and their morphology and contamination were regularly checked. For the experiments, only cells from passages 5–15 were utilized.[25]

MTT Assay

Based on mitochondrial metabolic activity, cell viability were evaluated by using the MTT [3-(4,5-dimethylthiazol-2-yl)-2,5-diphenyltetrazolium bromide] assay. In order to facilitate adhesion, cells were planted in 96-well plates at a density of 5,000–10,000 cells per well and incubated for the whole night. After that, different quantities of free doxorubicin, blank nanoparticles, or drug-loaded nanoparticles in full culture media were applied to the cells. As a negative control, untreated cells were used. Following treatment for 24, 48, and 72 hours, the media was taken out and each well was filled with MTT solution (5 mg/mL in PBS, diluted in culture medium to 0.5 mg/mL). Plates were incubated at 37°C for three to four hours so that live cells could generate formazan crystals. After the solution was thoroughly aspirated, the formazan crystals were dissolved by adding dimethyl sulfoxide (DMSO). A microplate reader (SpectraMax M3, Molecular Devices, USA) was used to measure the absorbance at 570 nm (with reference wavelength at 630 nm). The percentage of cell viability was computed in relation to untreated control cells, and nonlinear regression analysis was used to establish the IC_{50} values (concentration causing 50% inhibition of cell viability).[26]

SRB Assay

An additional method for calculating cell density using cellular protein concentration was the sulforhodamine B (SRB) assay. The MTT assay's instructions for seeding and treating cells were followed. After treatment, cells were fixed by adding cold trichloroacetic acid (TCA, final concentration 10%) and letting them sit at 4°C for an hour. The plates were air-dried after being repeatedly cleaned with deionized water. To enable the dye to bind to cellular proteins, SRB solution (0.4% w/v in 1% acetic acid) were added to the each well and allowed to sit at room temperature for half an hour. After washing with 1% acetic vinegar to remove any remaining dye, the plates were allowed to air dry. The protein-bound dye was dissolved with tris base solution (10 mM, pH 10.5), and absorbance were measured at 510 nm using a microplate reader. Dose-response curves were created to ascertain IC_{50} values, and cell survival was computed in relation to the untreated control.[27]

XTT Assay

An additional colorimetric test for evaluating cellular metabolic activity was the XTT [2, 3-bis-(2-methoxy-4-nitro-5-sulfophenyl)-2H-tetrazolium-5-carboxanilide] assay. Because there is no requirement for a solubilization phase, this assay has the benefit of directly forming a soluble formazan product. The MTT assay methodology was followed while seeding and treating the cells. Following the specified treatment period, the cell culture medium was immediately supplemented with the XTT labeling mixture, which was made in accordance with the manufacturer's instructions by mixing XTT solution with electron-coupling reagent. A plate was incubated in the dark at 37°C for two to four hours. Using a microplate reader, the absorbance of the orange formazan dye produced by metabolically active cell was measured at 450 nm with a reference wavelength of 650 nm. IC_{50} values and cell viability were computed using the previously mentioned method.[28]

Apoptotic Index Determination Using Trypan Blue (TB) Assay

By differentiating between viable cells (which exclude the dye) and non-viable cells (which take up the dye due to impaired membrane integrity), the trypan blue exclusion experiment was used to calculate the apoptotic index. Cell

was seeded in 6-well plates and exposed to drug-loaded nanoparticles or free doxorubicin at IC•³ concentrations for 24 and 48 hours. Both floating and adhering cells were gathered following treatment. Trypsin-EDTA was used to separate the adherent cells, which were then mixed with the floating cells and centrifuged. An aliquot of the cell pellet was combined with an equivalent volume of 0.4% trypan blue solution after it had been resuspended in PBS. Viable (unstained) and non-viable (blue-stained) cells were counted separately under a light microscope after the mixture was quickly put into a hemocytometer or automated cell counter. Each sample had a minimum of 200 cells counted. The formula was used to determine the apoptotic index:

Apoptotic Index (%) = (Number of non-viable cells / Total number of cells) × 100

Phase-contrast microscopy was also used to examine and record morphological changes such as cell shrinkage, typical of apoptosis, membrane blebbing, and the production of apoptotic bodies.[29]

Statistical Analysis

Every experiment was conducted at least three times, and the results were reported as either standard error of mean (SEM) or mean ± standard deviation (SD), depending on the situation. Using GraphPad Prism software (GraphPad Software, USA) statistical comparisons were carried out using one-way analysis of variance (ANOVA) followed by suitable post-hoc tests (Tukey's or Bonferroni) for multiple comparisons. At $p < 0.05$, differences were deemed statistically significant. Nonlinear regression analysis was used to calculate IC_{50} and concentration-response curves

RESULTS

Synthesis and Yield

Chitosan was effectively modified chemically with high reaction efficiency. With good yields and off-white to pale yellow powder, the refined modified chitosan demonstrated effective conversion and little product loss during purification. The color shift from native chitosan's white appearance indicated that the modifying group had been successfully introduced. When compared to native chitosan, the modified polymer showed better solubility properties, including improved dissolving in aqueous acidic conditions and maintenance of solubility over a wider pH range, which is beneficial for formulation development and biological applications. Characterization of Modified Chitosan

Elemental Analysis

Through CHN analysis, elemental analysis offered quantitative proof of effective chemical change. When the carbon, hydrogen, and nitrogen contents of native chitosan (F1) and modified chitosan samples (MF1 and MF2) were compared, clear compositional alterations that were consistent with the addition of functional groups were found (Table 1, Figure 1).

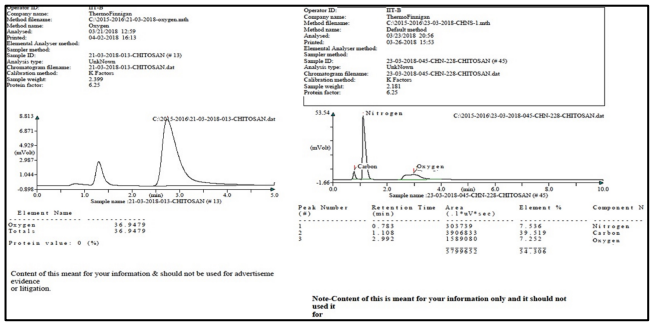

Fig. (1). CHN Analysis of Modified Chitosan

Table 1. CHN Analysis of Modified Chitosan

Sr. No.	Sample Name	N%	C%	H%	Sample Weight (mg)
1.	F1	7.14	38.43	8.04	10.10
2.	MF1	6.12	34.41	8.15	8.82
3.	MF2	6.99	38.78	6.96	5.45

FT-IR Spectroscopy Analysis

Chitosan's structural change was verified using FT-IR spectroscopy (Figure 2). O–H/N–H stretching (3200–3500 cm^{-1}), C–H stretching (2920–2870 cm^{-1}), amide I (≈1650 cm^{-1}), N–H bending (≈1590 cm^{-1}), and saccharide C–O–C vibrations (1150–1000 cm^{-1}) were all represented by distinctive bands in native chitosan. Successful chemical derivatization was demonstrated in the modified chitosan by the emergence of new absorption bands as well as shifts and intensity alterations in the amino and carbonyl regions. Crucially, the preservation of polysaccharide backbone peaks verified the integrity of the basic chitosan structure. These results confirmed the successful alteration of chitosan when combined with elemental analysis

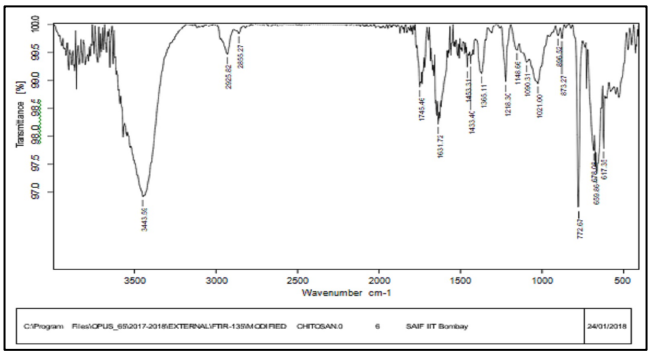

Fig. (2). FT-IR Spectroscopy of Modified Chitosan

Nuclear Magnetic Resonance (NMR) Spectroscopy The effective chemical derivatization of modified chitosan was validated by its ^{1}H NMR spectra (Figure 3). Anomeric protons (δ 4.5–5.0 ppm), pyranose ring protons (δ 3.0–4.0 ppm), and residual N-acetyl methyl groups (δ ≈ 2.0 ppm) were found to exhibit characteristic signals of the chitosan backbone. Significantly, new resonances that were not present in native chitosan emerged in areas that matched the functional moieties that were added, offering concrete proof of change. Site-specific derivatization was confirmed by shifts and splitting changes in the H-2 proton next to the amino group, indicating its participation in the reaction. The degree of substitution could be estimated in accordance with elemental analysis by integrating new peaks with respect to backbone protons, and the integrity of the backbone was validated by the preservation of distinctive chitosan signals.

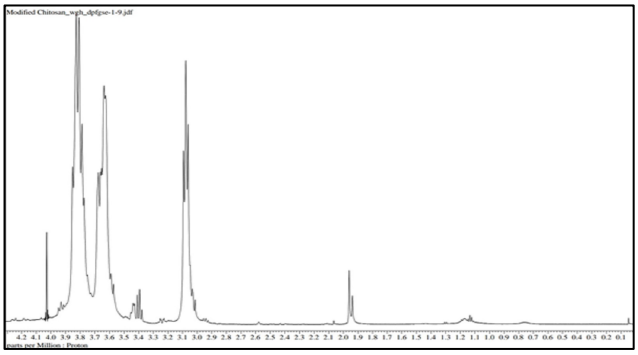

Fig. (3). 1H NMR spectrum of Modified Chitosan

Mass Spectrometry

The chemical alteration of chitosan was verified by ESI-MS analysis in negative ion mode (Figure 4). Analysis of oligomeric fragments showed well-resolved mass spectra, despite the polydispersity of entire chitosan polymers limiting direct detection. The inclusion of the grafted moiety resulted in systematic mass changes in the modified polymer when compared to native chitosan. Within the oligomeric range (m/z 200–2000), the measured m/z values and distinctive peak spacing matched the anticipated molecular weight increase of the modifying group. The spectroscopic results were corroborated by accurate mass and isotopic pattern analysis, which further showed effective grafting.

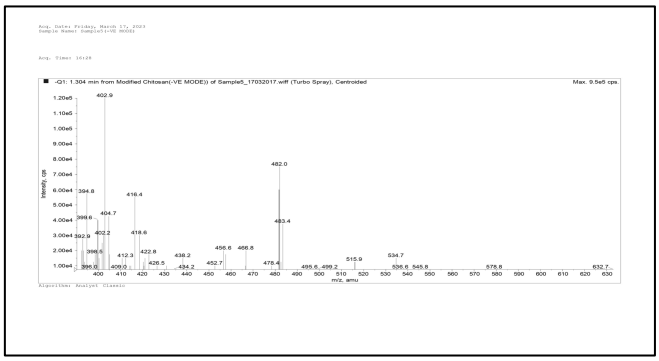

Fig. (4). Mass spectrometric analysis of Modified Chitosan

Quality by Design (QbD) Approach for Formulation Development

Risk Assessment and Identification of Critical Factors

Fishbone diagrams and FMEA were used in a systematic risk assessment to identify material characteristics and process parameters that could have a major impact on the CQAs of doxorubicin-loaded nanoparticles. Among the material attributes, modified chitosan concentration, TPP concentration, and doxorubicin concentration were identified as high-risk CMAs based on their expected influence on particle size, drug loading, and encapsulation efficiency. Because they control particle formation kinetics, size distribution, and repeatability, process variables such stirring speed, TPP addition rate, and stirring time were categorized as essential. This risk-based strategy made guaranteed that the most important variables were the focus of later experimental design, maximizing resource use and upholding scientific rigor. Based on this assessment, nine formulations (F1-F9) were prepared using varying concentrations of drug, modified chitosan, and TPP, as detailed in Table 2.

Table 2. Formulation Composition of Doxorubicin-Loaded Modified Chitosan Nanoparticles

Batch Code	Drug Doxorubicin(mg)	Modified Chitosan (mg)	Sodium Tripolyphosphate (mg)	Glacial Acetic Acid	Sodium Hydroxide (ml)

				(ml)	
F1	50	100	100	10	10
F2	50	50	50	10	10
F3	75	50	100	10	10
F4	100	75	50	10	10
F5	75	50	100	10	10
F6	100	100	100	10	10
F7	50	75	100	10	10
F8	50	100	75	10	10
F9	100	50	75	10	10

Design of Experiments and Response Surface Methodology

The impact of formulation and process factors on the crucial quality features of the nanoparticles were assessed using by Box-Behnken design. Particle size (Y_1) and zeta potential (Y_2) were chosen as the dependent responses and three levels of modified chitosan concentration (X_1), TPP concentration (X_2), and doxorubicin concentration (X_3) were examined. The data from nine randomly ordered experimental runs were fitted to second-order polynomial models. All three factors had a favourable impact, according to the particle size model, with changed chitosan concentration having the biggest impact. On the other hand, as chitosan, TPP, and medication concentration increased, zeta potential dropped, indicating improved ionic crosslinking and surface charge regulation. Both models showed strong correlations between expected and experimental results, with high coefficients of determination ($R^2 > 0.90$). The robustness of the model was proven by the good match between the expected and modified R2. The models' suitability for optimization and design space exploration was confirmed by the ANOVA findings, which revealed statistically significant models ($p < 0.05$) with non-significant lack of fit:

A. Polynomial Equation for Particle Size (Y_1)

$$\sqrt{Y1} = 14.9373 + 1.3948A + 0.4667B + 0.1826C$$

Where A = modified chitosan concentration, B = TPP concentration, and C = doxorubicin concentration.

B. Polynomial Equation for Zeta Potential (Y_2)

$$Y2 = -14.6909 - 0.7912A - 2.1425B - 2.3216C$$

High coefficients of determination ($R^2 > 0.90$ for all responses) were found in the statistical evaluation of the created models, suggesting that the models sufficiently explained the variability found in the experimental data. The models' strong predictive performance was further supported by the excellent agreement between the adjusted R2 and anticipated R2 values. The models' statistical significance ($p < 0.05$) and non-significant lack-of-fit values were confirmed by analysis of variance (ANOVA), confirming their appropriateness for investigating and traversing the formulation design space.[35]

Effect on Particle Size (Y_1)

The greatest regression coefficient (+1.3948) indicates that the modified chitosan concentration had the strongest beneficial influence on particle size. Particle size increased noticeably when polymer concentration was increased from 0.5 to 1.5 mg/mL, which was caused by increased solution viscosity and more polymer chains available for ionic crosslinking. Batches with higher chitosan levels (e.g., F6 and F8) produced larger particles than those with lower polymer concentration (F2, F3, and F5). This pattern was consistently seen throughout formulations. Additionally, TPP concentration had a positive but relatively lesser effect on particle size (coefficient = +0.4667), indicating increased crosslinking density at higher crosslinker concentrations. However, differences across formulations with different doses of TPP and chitosan showed that its effect was highly reliant on the polymer–crosslinker ratio. On the other hand, doxorubicin concentration had only a slight impact on particle size (coefficient = +0.1826), suggesting that drug loading had little effect on particle growth within the range under investigation.

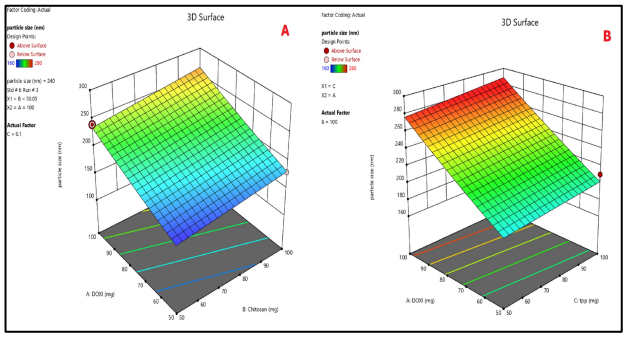

Fig. (5). A) Three-dimensional response surface plot Chitosan vs Doxorubicin for particle size response. B) Three-dimensional response surface plot TPP vs Doxorubicin particle size response

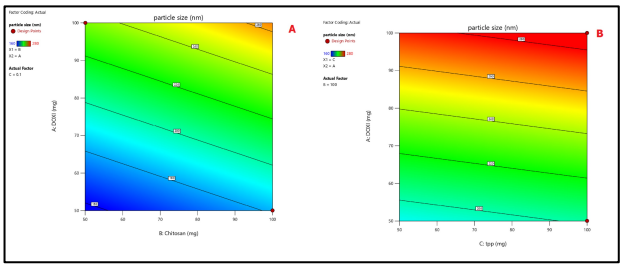

Fig. (6). A) Two-dimensional contour plots Chitosan vs Doxorubicin for particle size response. B) Two-dimensional contour plots TPP vs Doxorubicin particle size response.

Effect on Zeta Potential (Y_2)

All formulation factors had a significant impact on zeta potential, with progressive surface charge neutralization indicated by negative coefficients. Because of increased ionic contact with TPP at higher polymer levels, modified chitosan concentration had a slight negative effect (−0.7912). Increased crosslinking successfully decreased surface positivity through phosphate–amine interactions, as demonstrated by the highest effect of TPP concentration (−2.1425). Zeta potential was also adversely influenced by doxorubicin concentration (−2.3216), most likely as a result of interactions with surface amino groups and modification of polymer conformation during nanoparticle formation.

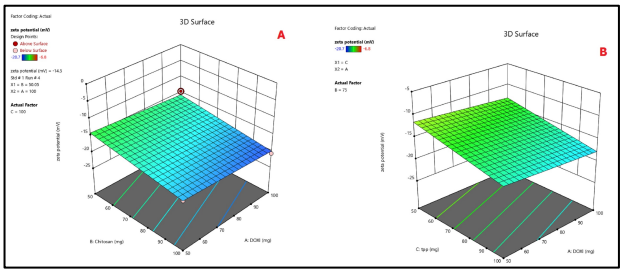

Fig. (7). A) Three-dimensional response surface plot Chitosan vs Doxorubicin for zeta potential response. B) Three-dimensional response surface plot TPP vs Doxorubicin zeta potential.

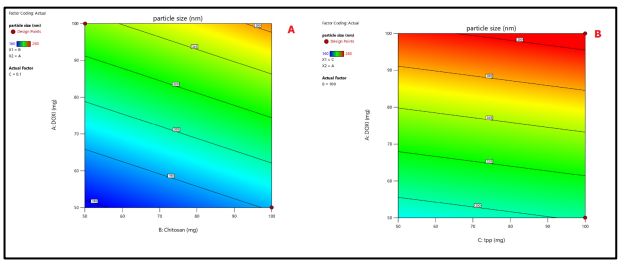

Fig. (8). A) Two-dimensional contour plots Chitosan vs Doxorubicin for zeta potential response. B) Two-dimensional contour plots TPP vs Doxorubicin zeta potential response.

Physicochemical Characterization of Nanoparticles

Particle Size, Polydispersity Index (PDI), and Zeta Potential

DLS research revealed that the improved formulation F1 has outstanding physicochemical attributes (Figures 9 and 10). With a very low PDI of 0.019 and a mean z-average diameter of 223.4 nm, the nanoparticles demonstrated a very monodisperse system. As of the improved permeability and retention (EPR) effect, this size range is advantageous for intravenous delivery and tumor accumulation. The homogeneity and lack of aggregation were confirmed by the DLS profile, which showed a crisp, unimodal distribution with >95% of particles around the mean size. Enough electrostatic repulsion was given by the zeta potential of −25.3 mV to ensure colloidal stability. Size and zeta potential did not significantly alter after 30 days of stability testing at 4 °C (CV < 3%). The robustness of the formulation technique was confirmed by the same properties of blank nanoparticles.

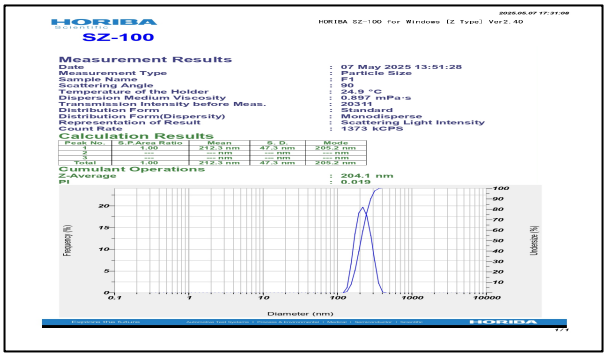

Fig. (9). Particle Size Analysis of optimized batch F01

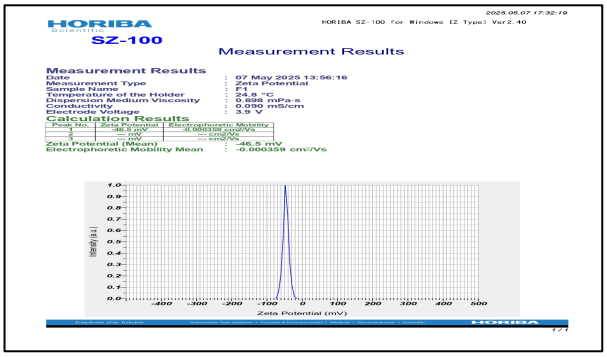

Fig. (9). Zeta Potential Analysis of optimized batch F01

Encapsulation Efficiency and Drug Loading

With an efficiency of 88.04 ± 1.53% and drug loading of 7.52 ± 0.15% (Table 3, Figures 11–12), the improved formulation F1 outperformed all other formulations in terms of drug encapsulation. Efficient doxorubicin entrapment inside the nanoparticle matrix is reflected in high encapsulation, which reduces drug loss and increases therapeutic potential. The key to optimizing encapsulation was a higher modified chitosan content (100 mg) and an ideal polymer-to-drug ratio (100:50), underscoring the crucial significance of formulation parameters in attaining clinically meaningful drug delivery with low injected volume.[37]

Table 3. Encapsulation Efficiency and Drug Loading Results

Batch No.	Modified Chitosan (mg/mL)	TPP (mg/mL)	Stirring Speed (rpm)	Encapsulation Efficiency (%)	Drug Loading (%)
F1	1.0	0.6	1000	88.04 ± 1.53	7.52 ± 0.15
F2	1.5	0.3	1000	81.45 ± 2.07	6.84 ± 0.22
F3	0.5	0.9	1000	72.49 ± 2.64	4.58 ± 0.16
F4	1.5	0.9	1000	78.12 ± 1.94	6.12 ± 0.19
F5	0.5	0.6	500	69.86 ± 2.51	4.39 ± 0.21
F6	1.5	0.6	500	84.94 ± 1.69	7.18 ± 0.24
F7	0.5	0.6	1500	63.96 ± 2.93	4.05 ± 0.19
F8	1.5	0.6	1500	77.60 ± 2.00	6.43 ± 0.20
F9	1.0	0.3	500	74.97 ± 2.24	5.64 ± 0.18

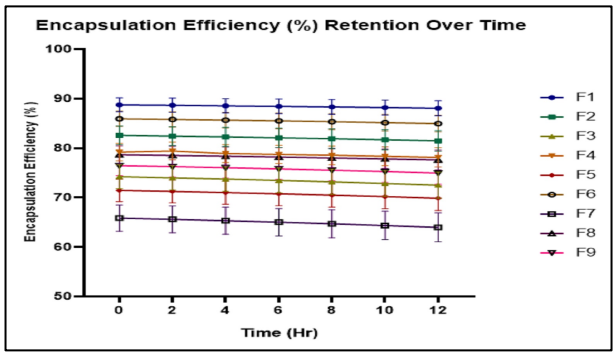

Fig. (11). Encapsulation efficiency (%) of modified chitosan nanoparticles prepared using Box–Behnken design. Data are expressed as mean ± SD (n = 3). Batches F01–F09 represents centre point formulations.

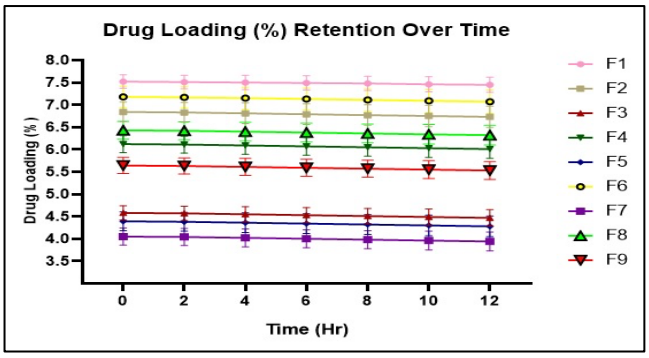

Fig. (12). Retention of drug loading (%) of modified chitosan nanoparticle formulations (F1–F9) during storage at 4 °C protected from light. Values represent mean ± SD (n = 3).

Differential Scanning Calorimetry (DSC)

Important information about the physical state of doxorubicin and drug-polymer interactions within nanoparticles was revealed by differential scanning calorimetry (DSC). The crystalline nature of pure doxorubicin hydrochloride was demonstrated by a strong endothermic peak at around 205–210°C. Broad dehydration peaks (~100–115°C) and degradation transitions above 280°C were seen in both native and modified chitosan, with slight changes in modified chitosan indicating chemical derivatization. The drug's melting peak (~208°C) was preserved in the physical combination of doxorubicin and modified chitosan, suggesting no substantial solid-state interaction without the production of nanoparticles. On the other hand, doxorubicin's melting peak completely vanished in the improved formulation F1, indicating molecular-level dispersion or amorphous inclusion inside the polymer matrix. With just dehydration (~110°C) and degradation (>280°C) peaks, the thermogram resembled modified

chitosan and demonstrated exceptional thermal stability. While stability above 250°C guarantees compatibility for processing, storage, and sterilization, loss of crystallinity indicates improved solubility, bioavailability, and sustained release potential. The modified chitosan was mirrored by blank nanoparticles, indicating that the crosslinking process maintains matrix integrity.[39]

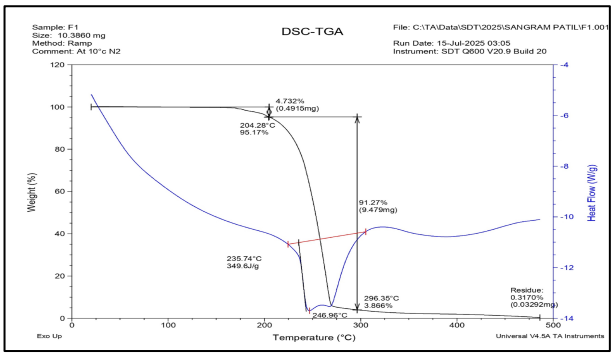

Fig. (13). DSC thermograms of doxorubicin, modified chitosan, and F1 nanoparticles, showing disappearance/shift of the drug's melting peak, indicating successful encapsulation and reduced crystallinity

X-ray Diffraction (XRD)

The physical condition of doxorubicin in the nanoparticles was confirmed by X-ray diffraction (XRD) analysis, which supported the DSC results (Figure 14). The highly crystalline nature of pure doxorubicin hydrochloride was demonstrated by its prominent, powerful peaks at distinctive 2θ values (10.2°, 12.8°, 15.6°, 18.4°, 20.8°, 22.4°, and 24.6°). Around 19–20°, modified chitosan showed a wide, amorphous halo that is typical of semicrystalline polysaccharides. Doxorubicin's crystalline peaks were preserved in the physical mixture, suggesting that drug crystallinity is not affected by straightforward mixing. On the other hand, the optimized F1 nanoparticles demonstrated molecular-level dispersion of doxorubicin within the polymer matrix, with a diffractogram resembling amorphous chitosan and full elimination of all drug diffraction peaks. Intimate drug-polymer interactions, such as hydrogen bonding, electrostatic attraction, and physical entrapment, are confirmed by this transition from crystalline to amorphous form. Strong proof of effective encapsulation and the creation of a real solid solution appropriate for regulated drug administration is provided by the molecular dispersion, which improves solubility, bioavailability, and sustained release.

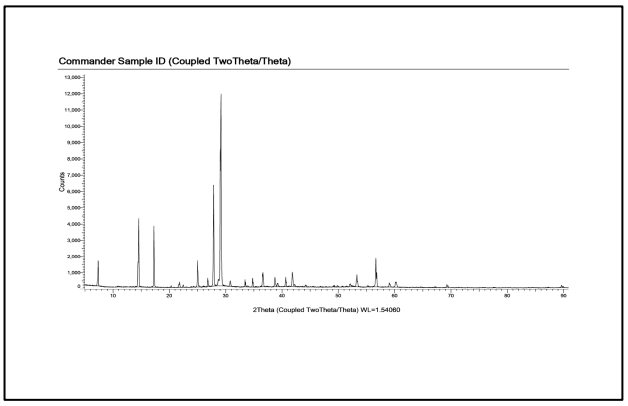

Fig. (14). XRD patterns of pure drug, modified chitosan, and optimized formulation (F1) show disappearance of the drug's crystalline peaks in F1, confirming its amorphous or molecularly dispersed state within the nanoparticles

Scanning Electron Microscopy (SEM)

A field emission scanning electron microscope (FESEM, JSM-In line with DLS results (223.4 ± 5 nm, PDI 0.019), SEM analysis of lyophilized F1 nanoparticles (Figure 15) showed primarily spherical to slightly oval particles with smooth surfaces and uniform size (180–250 nm). During freeze-drying, trehalose successfully inhibited fusion, and loose aggregates were readily redispersible. DSC/XRD results were supported by the absence of surface drug crystals, which confirmed full encapsulation in an amorphous condition. With ideal biodistribution and colloidal stability, the dense, smooth matrix implies sustained release, controlled drug diffusion, and parenteral administration appropriateness.

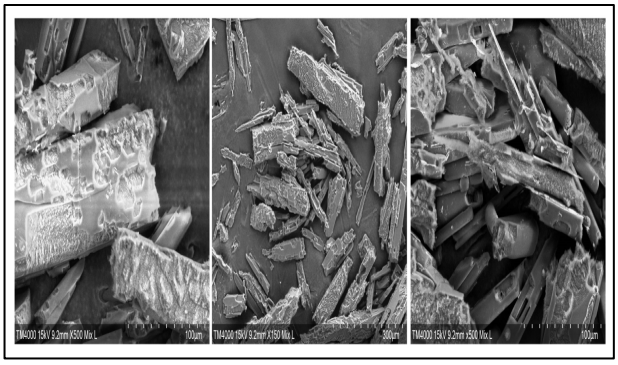

Fig. (15). SEM image of F1 nanoparticles showing uniform, spherical particles with smooth surfaces, confirming successful formation using modified chitosan

Transmission Electron Microscopy (TEM) Consistent with DLS and SEM data, TEM analysis of F1 nanoparticles (Figure 16) showed well-defined, mostly spherical particles

with uniform size (~218 ± 12 nm) and smooth surfaces. According to DSC and XRD, the nanoparticles had a homogeneous internal structure with a moderate electron density, no crystalline domains, and support for doxorubicin molecular dispersion. Subtle core-shell contrast was seen in some particles, indicating progressive drug concentration gradients without phase separation. The stability and structural integrity of the particles were confirmed by their discreteness and lack of aggregation. All things considered, TEM verified uniform size, spherical morphology, smooth surface, and amorphous drug encapsulation, emphasizing appropriateness for tumor-targeted therapy via the EPR effect and regulated parenteral drug delivery.

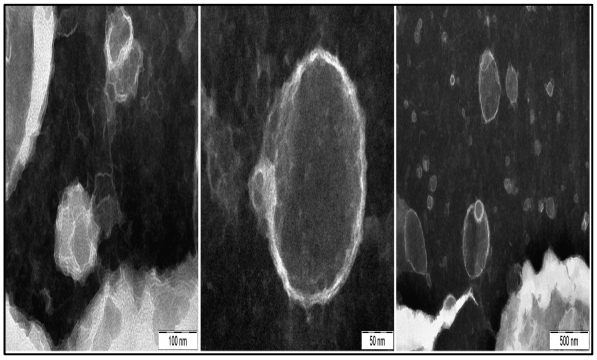

Fig. (16). TEM image of F1 nanoparticles showing discrete, spherical particles with well-defined boundaries at the nanoscale, confirming SEM-observed morphology.

***In-Vitro* Drug Release Studies:**

The release kinetics of doxorubicin from the nanoparticles and the formulation's capacity to give sustained drug delivery under physiologically relevant conditions were assessed using in vitro drug release tests. Two pH levels were used for release studies: pH 5.5 (acetate buffer modelling the acidic tumor microenvironment and endosomal/lysosomal compartments) and pH 7.4 (phosphate-buffered saline replicating blood pH and normal tissue environment).

Drug Release at pH 7.4 (Physiological Conditions)

A clear biphasic pattern typical of matrix-type controlled release systems was shown by the cumulative percent release profiles at pH 7.4 (Figure 17, Table 4). Within the first two to four hours, all formulations showed an initial phase of rather rapid release, which represented the release of drug molecules that were close to or at the particle surface and easily accessible to the dissolving solvent. The medication gradually diffused from the inside of the crosslinked polymer matrix after this, as evidenced by a longer, slower release phase that lasted for 12 hours.

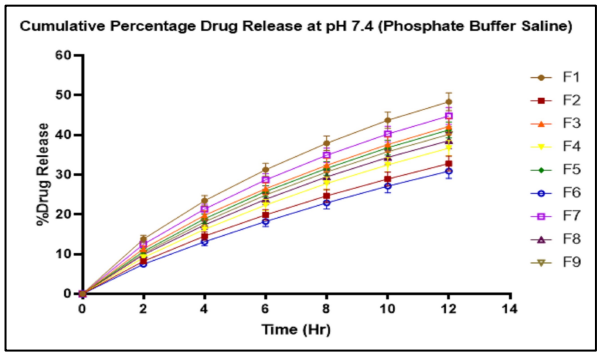

Fig. (17). Cumulative drug release of F1–F9 nanoparticles in PBS (pH 7.4), showing the effects of chitosan concentration, TPP concentration, and stirring speed on release kinetics (mean ± SD, n = 3).

Table 4. Cumulative Drug Release at pH 7.4 (12 hours)

Batch	0 hr	2 hr	4 hr	6 hr	8 hr	10 hr	12 hr
F1	0	7.12 ± 0.58	12.45 ± 0.95	17.34 ± 1.25	21.78 ± 1.48	25.89 ± 1.68	29.56 ± 1.82
F2	0	8.23 ± 0.65	14.56 ± 1.05	19.89 ± 1.34	24.67 ± 1.58	28.92 ± 1.76	32.78 ± 1.89
F3	0	11.34 ± 0.82	19.78 ± 1.18	26.45 ± 1.48	32.34 ± 1.71	37.56 ± 1.88	42.12 ± 2.05
F4	0	9.12 ± 0.71	16.23 ± 1.12	22.34 ± 1.41	27.78 ± 1.63	32.45 ± 1.82	36.67 ± 1.96
F5	0	10.67 ± 0.78	18.89 ± 1.15	25.78 ± 1.45	31.56 ± 1.68	36.78 ± 1.86	41.23 ± 2.02
F6	0	7.45 ± 0.61	13.12 ± 0.98	18.23 ± 1.28	22.89 ± 1.52	27.12 ± 1.71	30.89 ± 1.85
F7	0	13.78 ± 0.94	23.45 ± 1.31	31.23 ± 1.64	37.89 ± 1.85	43.67 ± 2.08	48.34 ± 2.24
F8	0	9.89 ± 0.73	17.34 ± 1.14	23.78 ± 1.43	29.45 ± 1.67	34.34 ± 1.84	38.56 ± 1.98
F9	0	10.23 ± 0.76	18.12 ± 1.16	24.89 ± 1.46	30.67 ± 1.69	35.78 ± 1.87	40.12 ± 2.01
Free	0	68.45	87.34	94.67	97.23	98.56	99.12

Drug		± 3.21	± 2.89	± 2.45	± 2.12	± 1.89	± 1.67

In contrast to >99% release from free drug within 8 hours, the improved F1 formulation showed a sustained release profile, releasing only 29.56 ± 1.82% of doxorubicin over 12 hours at pH 7.4. This approximately 70% decrease validates successful encapsulation and shows how the modified chitosan matrix can regulate drug release.

Effect of Chitosan Concentration

Drug release was reduced by higher chitosan concentrations (100 mg), with F1 and F6 releasing 29.56% and 30.89% as opposed to 32.78–42.12% from lower polymer formulations (F2, F3, F5, F9), indicating a denser matrix and increased diffusional resistance. By forming stronger crosslinked networks, a higher TPP concentration (100 mg) further prolonged release. The effects of drug loading were complicated; increased loading (F4, F6, F9) did not consistently speed up release, probably because of improved drug-polymer interactions. Due to a less dense polymer matrix despite significant crosslinking, F7 (50 mg medication, 75 mg chitosan, 100 mg TPP) showed the fastest release (48.34% at 12 h). Longer tumor-site drug exposure, lower peak plasma toxicity, fewer doses, and increased tumor accumulation through the EPR effect are among the therapeutic benefits of sustained release of F1.

Drug Release at pH 5.5 (Tumor Microenvironment)

Release studies at acidic pH (5.5) revealed pronounced pH-responsive behavior (Figure 18, Table 5), with all formulations demonstrating significantly enhanced release rates compared to pH 7.4.

Table 5. Cumulative Drug Release at pH 5.5 (12 hours))

Batch	0 hr	2 hr	4 hr	6 hr	8 hr	10 hr	12 hr
F1	0	11.67 ± 0.91	20.89 ± 1.36	28.78 ± 1.74	35.45 ± 1.98	41.34 ± 2.18	46.34 ± 2.35
F2	0	13.45 ± 0.98	23.78 ± 1.45	32.12 ± 1.84	39.23 ± 2.08	45.34 ± 2.28	50.67 ± 2.45
F3	0	17.23 ± 1.08	29.67 ± 1.62	39.12 ± 1.95	47.01 ± 2.22	53.67 ± 2.42	59.34 ± 2.61
F4	0	14.78 ± 1.02	25.89 ± 1.52	34.78 ± 1.88	42.12 ± 2.13	48.45 ± 2.33	53.89 ± 2.51
F5	0	16.45 ± 1.06	28.34 ± 1.58	37.67 ± 1.92	45.56 ± 2.18	52.23 ± 2.38	57.78 ± 2.57
F6	0	12.23 ± 0.94	21.67 ± 1.39	29.89 ± 1.78	36.78 ± 2.01	42.89 ± 2.21	48.12 ± 2.38
F7	0	19.89 ± 1.18	33.78 ± 1.76	44.12 ± 2.08	52.67 ± 2.36	59.78 ± 2.58	65.67 ± 2.78
F8	0	15.67 ± 1.04	27.12 ± 1.55	36.45 ± 1.90	44.23 ± 2.16	50.89 ± 2.37	56.45 ± 2.55
F9	0	16.12 ± 1.05	27.89 ± 1.57	37.23 ± 1.91	45.12 ± 2.17	51.78 ± 2.38	57.34 ± 2.56
Free Drug	0	71.23 ± 3.34	89.67 ± 2.98	95.89 ± 2.56	98.12 ± 2.23	99.01 ± 1.95	99.45 ± 1.78

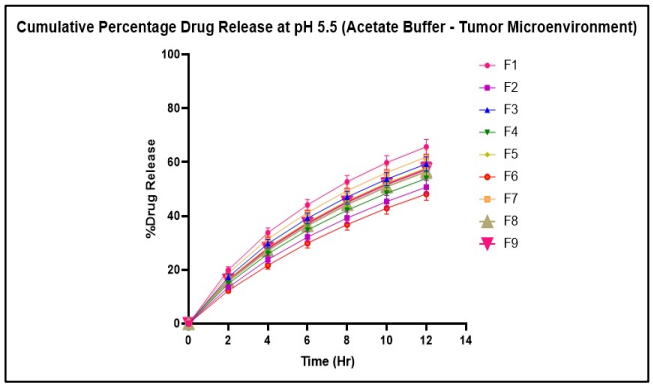

Fig. (18). Cumulative drug release of F1–F9 nanoparticles in acetate buffer (pH 5.5) over 12 h, showing enhanced, pH-responsive release (mean ± SD, n = 3).

Over the course of 12 hours, Formulation F1 released 46.34 ± 2.35% of doxorubicin at pH 5.5, a 1.57-fold increase over pH 7.4 (29.56%), demonstrating the pH-responsive behavior seen in all formulations (enhancement 1.5–1.7×). Chitosan amino groups are protonated by acidic pH, which accelerates release by producing polymer chain repulsion, network expansion, weaker crosslinking, improved hydration, and greater drug solubility. This tumor-selective release improves intracellular delivery while reducing systemic exposure and toxicity by favoring higher drug concentrations in endosomal compartments and acidic tumor microenvironments.[40]

Release Kinetics and Mechanism:

The Korsmeyer-Peppas model best explained the release of doxorubicin from F1 (R^2 = 0.9823 at pH 7.4; 0.9856 at pH 5.5), with release exponents n = 0.58 (pH 7.4) and n = 0.64 (pH 5.5), showing anomalous (non-Fickian) transport. This explains the observed biphasic release through a combination process of polymer chain relaxation/erosion and Fickian diffusion. Increased polymer swelling and chain repulsion are reflected in the greater n at acidic pH, which is consistent with pH-responsive behavior. Simple constant-rate or concentration-driven release was ruled out by poor fits to zero- and first-order models, but diffusion's important role was verified by a reasonable Higuchi correlation (R^2 = 0.9234). These results show that F1 provides sustained, pH-responsive kinetics for regulated, tumor-targeted drug delivery.

I*n Vitro* Anticancer Activity:

Cytotoxicity Assessment Using Multiple Assays

An MTT, SRB, and XTT assay was to examine the anticancer activity of doxorubicin-loaded F1 nanoparticles, offering a reliable, multi-assay evaluation of cellular viability and proliferation. This alternative strategy minimizes method-specific artifacts while guaranteeing accurate assessment of cytotoxic potential.

MTT Assay Results

Cell viability was evaluated in MCF-7 breast adenocarcinoma cells after treatment with free drug (5-fluorouracil used as standard), blank nanoparticles (control), and the optimized doxorubicin-loaded formulation F1 using the MTT assay, which measures mitochondrial metabolic activity through reduction of tetrazolium salt by mitochondrial dehydrogenases (Table 6, Figures 19-20).

Table 6. IC_{50} values from MTT assay for standard drug, doxorubicin-loaded nanoparticles (F1), and control, expressed as mean ± SD (n = 3); statistical significance analyzed by one-way ANOVA with post-hoc tests.

Sr. No.	Sample Code	Conc. (µg/ml)	OD			Mean	% of Inhibition	% of Viability	IC 50 (µg/ml)
1	Control	100	1.482			1.482	0	-	-
2	Standard (5,Fluro ur-acil)	20	0.916	0.915	0.916	0.915 ± 0.001	38.25	61.75	49.33
		40	0.732	0.729	0.734	0.731 ± 0.002	50.67	49.33	
		60	0.507	0.504	0.502	0.504 ± 0.003	65.9	34.01	
		80	0.315	0.312	0.314	0.313 ± 0.002	78.87	21.13	
		100	0.208	0.205	0.207	0.206 ± 0.002	86.09	13.91	
3	Formulation	20	1.069	1.065	1.071	1.068 ± 0.003	27.93	72.07	70.69
		40	0.945	0.944	0.942	0.943 ± 0.002	36.36	63.64	
		60	0.761	0.763	0.756	0.76 ± 0.004	48.71	51.29	
		80	0.604	0.601	0.606	0.603 ± 0.003	59.31	40.69	
		100	0.489	0.485	0.493	0.489 ± 0.004	67.00	33.00	

The conventional medication (5-fluorouracil) and F1 nanoparticles both showed concentration-dependent cytotoxicity in the MTT experiment. With an IC^{21} of 49.33 µg/mL and an 86.09% growth inhibition at 100 µg/mL, the standard medication demonstrated strong action. With an IC^{21} of 70.69 µg/mL, F1 demonstrated significant anticancer activity, lowering cell viability to 33% at 100 µg/mL, indicating the duration needed for intracellular drug release and nanoparticle absorption. F1 had a highly linear dose-response (R2 = 0.9845) and >48% growth inhibition at >60 µg/mL. In F1-treated cells, microscopy verified distinctive cytotoxic morphological alterations, such as cell rounding, detachment, and fragmentation, which are comparable to typical medication effects. Blank nanoparticles and control cells both maintained >95% viability, indicating that doxorubicin, not the polymer carrier, was responsible for the cytotoxicity.

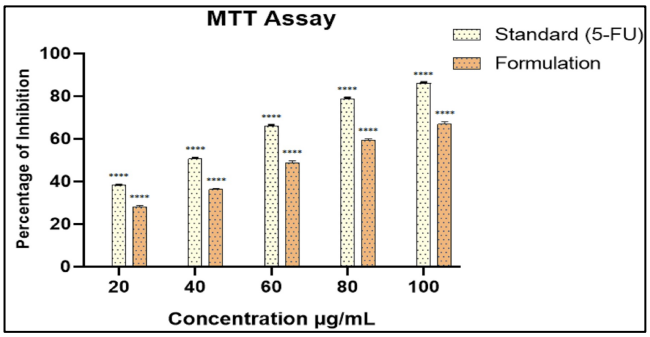

Fig. (19). MTT assay showing concentration-dependent cytotoxicity of 5-FU and F1 nanoparticles in MCF-7 cells (20–100 µg/mL); data expressed as mean ± SD (n = 3), with statistical significance by one-way ANOVA and post-hoc tests

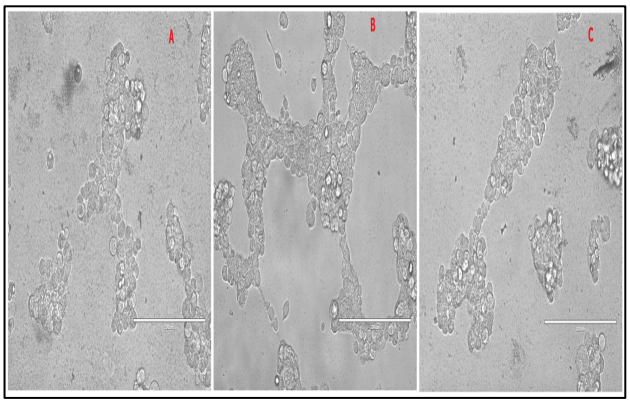

Fig. (20). Phase-contrast images of MCF-7 cells after IC_{50} treatment: (A) control with normal morphology, (B) 5-FU showing cytotoxic effects, and (C) F1 nanoparticles exhibiting apoptotic features; scale bar = 200 µm

SRB Assay Results

To supplement and validate MTT data (Table 7, Figures 21–22), the SRB assay were used to measure total cellular protein as a measure of cell density and proliferation. This assay provides an evaluation that is independent of metabolic activity.

Table 7. SRB assay showing concentration-dependent cytotoxicity of control, 5-FU, and F1 nanoparticles in MCF-7 cells, summarizing OD, mean OD, % inhibition, % viability, and IC_{50} (20–100 µg/mL).

Sr. No.	Sample Code	Conc. (µg/ml)	OD	Mean	% of Inhibition	% of Viability	IC 50 (µg/ml)
1	Control	20	1.069	1.065	1.071	1.068	27.93	72.07	70.69
		40	0.945	0.944	0.942	0.943	36.36	63.64	
		60	0.761	0.763	0.756	0.76	48.71	51.29	
		80	0.604	0.601	0.606	0.603	59.31	40.69	
		100	0.489	0.485	0.493	0.489	67.00	33.00	
2	Standard (5,Flurour-acil)	20	0.96	0.97	0.98	0.97	37.01	62.99	31.5
		40	0.72	0.72	0.71	0.71	53.89	46.11	
		60	0.32	0.34	0.32	0.32	79.22	20.78	
		80	0.25	0.25	0.25	0.25	83.37	16.63	
		100	0.19	0.19	0.19	0.19	87.66	12.34	
3	Formulation	20	1.42	1.45	1.38	1.41	8.44	91.56	81.11
		40	1.25	1.22	1.25	1.24	19.48	80.52	
		60	0.95	0.99	0.96	0.96	37.66	62.34	
		80	0.81	0.79	0.82	0.8	48.05	51.95	
		100	0.6	0.63	0.63	0.62	59.74	40.26	

The SRB assay confirmed concentration-dependent cytotoxicity of F1, corroborating MTT results. The standard drug exhibited an IC_{50} of 31.50 µg/mL with 87.66% growth inhibition at 100 µg/mL, while F1 showed an IC_{50} of 81.11 µg/mL and 59.74% inhibition, reflecting dose-dependent antiproliferative activity. Close agreement between MTT and SRB validates genuine cytotoxic effects rather than assay-specific artifacts. Microscopy revealed pronounced morphological changes: F1-treated cells displayed rounding, detachment, membrane blebbing, and apoptotic bodies,

while controls remained healthy. The progressive protein depletion indicates apoptotic cell death and effective growth inhibition, highlighting the therapeutic potential of the nanoformulation.[41]

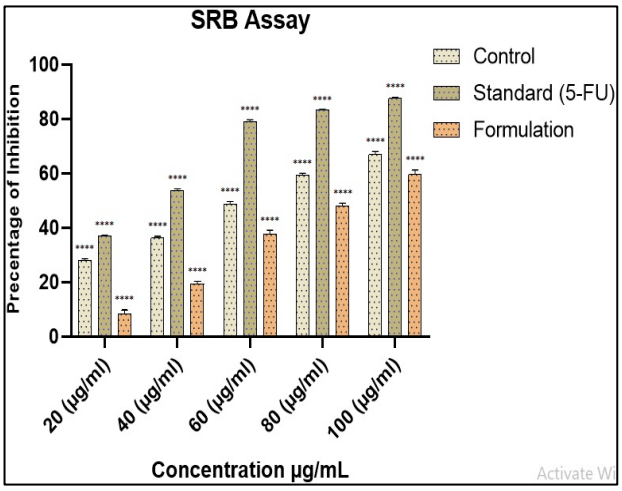

Fig. (21). SRB assay showing dose-dependent antiproliferative effects of control, 5-FU, and F1 nanoparticles in MCF-7 cells (20–100 µg/mL), with IC_{50} values corroborating MTT results and data expressed as mean ± SD (n = 3).

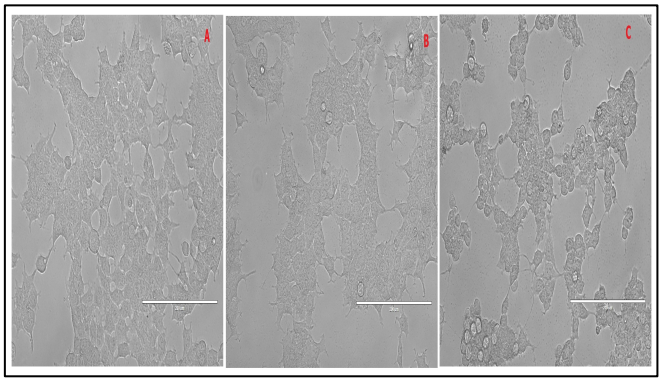

Fig. (22). Phase-contrast images of MCF-7 cells: (A) control with normal morphology, (B) 5-FU showing moderate cytotoxicity, and (C) F1 nanoparticles exhibiting pronounced apoptotic features; scale bar = 200 µm.

XTT Assay Results

The XTT assay, another metabolic activity assay based on tetrazolium reduction but forming soluble formazan product, was employed as a third independent confirmation of anticancer efficacy (Table 8, Figures 23-24). This assay offers advantages of direct formation of soluble formazan, eliminating the solubilization step required for MTT.

Table 8. XTT assay results showing OD, % inhibition, % viability, and IC_{50} for control, 5-FU, and F1 nanoparticles in MCF-7 cells at varying concentrations.

Sr. No.	Sample Code	Conc. (µg/ml)	OD			Mean	% of Inhibition	% of Viability	IC 50 (µg/ml)
1	Control	25	0.968	0.965	0.968	0.968	3.2	96.8	
		50	0.962	0.959	0.962	0.962	3.8	96.2	
		75	0.959	0.956	0.959	0.959	4.1	95.9	70.69
		100	0.955	0.951	0.955	0.955	4.5	95.5	
		125	0.95	0.946	0.95	0.95	5	95	
2	Standard (5,Flurour-acil)	25	0.977	0.975	0.979	0.977	36.31	63.69	
		50	0.746	0.744	0.748	0.746	51.36	48.64	38.12
		75	0.519	0.521	0.518	0.519	66.16	33.84	
		100	0.389	0.389	0.387	0.388	74.70	25.30	
		125	0.246	0.248	0.244	0.246	83.96	16.04	
3	Formulation	25	1.402	1.398	1.408	1.402	5.40	94.60	
		50	1.295	1.296	1.292	1.294	12.69	87.31	NE
		75	1.101	1.109	1.107	1.105	25.44	74.56	

		100	0.887	0.889	0.882	0.886	40.22	59.78	
		125	0.782	0.786	0.78	0.782	47.23	52.77	

Values represent mean ± SD (n = 3). **p < 0.01, ***p < 0.001 vs. control (one-way ANOVA followed by Tukey's post-hoc test)

*NE = Not Evaluable at tested concentration range; IC_{50} > 125 µg/mL

Consistent with MTT and SRB results, the XTT assay verified F1's concentration-dependent cytotoxicity. F1 exhibited 47.23% inhibition at the same dose, indicating slower intracellular absorption and drug release, whereas the conventional medication demonstrated an IC^{21} of 38.12 µg/mL with 83.96% inhibition at 125 µg/mL. Repeatable cytotoxic effects were shown by extremely linear dose-response curves (R2 = 0.9756). Assays have different objectives (mitochondrial activity, protein content, and metabolic activity), which are reflected in differences in IC_{20} values. Microscopy confirmed gradual, apoptosis-like cytotoxicity by showing F1-induced cell rounding, detachment, and decreased viability. Overall, F1 demonstrated significant and consistent anticancer activity that was confirmed by three complementary assays.

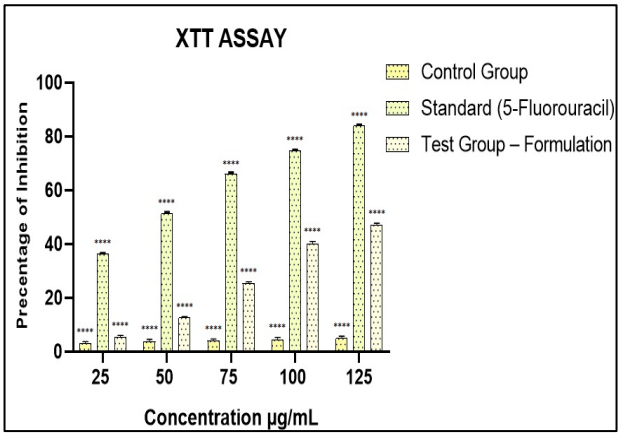

Fig. (23). XTT assay showing concentration-dependent cytotoxicity of control, 5-FU, and F1 nanoparticles in MCF-7 cells (25–125 µg/mL); data expressed as mean ± SD (n = 3), **p < 0.0001.

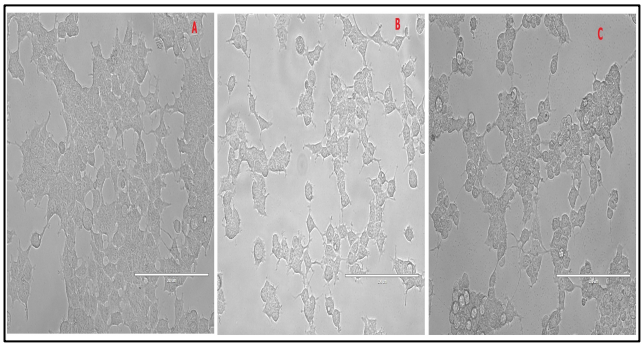

Fig. (24). Phase-contrast images of MCF-7 cells after XTT assay: (A) control with normal morphology, (B) 5-FU showing cytotoxic changes, and (C) F1 nanoparticles exhibiting moderate cell shrinkage and reduced viability; scale bar = 200 µm.

Comparative Analysis

The mechanistic advantages of F1 nanoparticles are highlighted by statistical comparison of IC·₀ values across MTT, SRB, and XTT experiments. While maintaining therapeutic intracellular concentrations over time, reduced apparent potency in comparison to free drug is explained by slower initial absorption via endocytosis and pH-triggered intracellular release. By avoiding efflux pumps, nanoparticle distribution guarantees improved drug retention and all-encompassing cytotoxic effects, such as decreased biomass, altered metabolic activity, and mitochondrial dysfunction. Prolonged intracellular exposure in conjunction with EPR-mediated tumor accumulation indicates the promise of F1 as a useful anticancer therapy, and the ICβ¹ range (70–80 µg/mL) is therapeutically meaningful.

Apoptotic Index Determination

The apoptotic index and the mechanism of cell death caused by F1 nanoparticles were evaluated using the trypan blue exclusion assay. Unlike necrosis, apoptosis eradicates cancer cells without causing inflammation. After 48 hours of treatment with IC•¹ concentrations of 5-FU or F1, MCF-7 cells were stained with 0.4% trypan blue, which only penetrates cells with damaged membranes. The percentage of blue-stained non-viable cells in relation to total cells was used to generate the apoptotic index (Figure 25& 26, Table 9), which sheds light on the cytotoxicity caused by nanoparticles.

Table 9. Apoptotic Index Results

Treatment	Viable Cells	Non-Viable Cells	Total Cells	Apoptotic Index (%)

Control	287 ± 12	13 ± 3	300	4.33 ± 1.00
Standard (5-FU)	142 ± 18	158 ± 18	300	52.67 ± 6.00**
Formulation F1	168 ± 15	132 ± 15	300	44.00 ± 5.00**
Control	287 ± 12	13 ± 3	300	4.33 ± 1.00

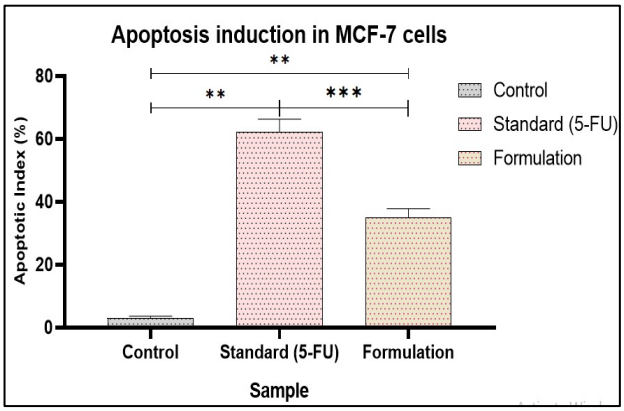

Fig. (25). Apoptotic index (%) in MCF-7 cells after treatment with control, 5-FU, and F1 nanoparticles, showing significant apoptosis induction by the drug and formulation (mean ± SD, n = 3; **p < 0.01, *p < 0.001).

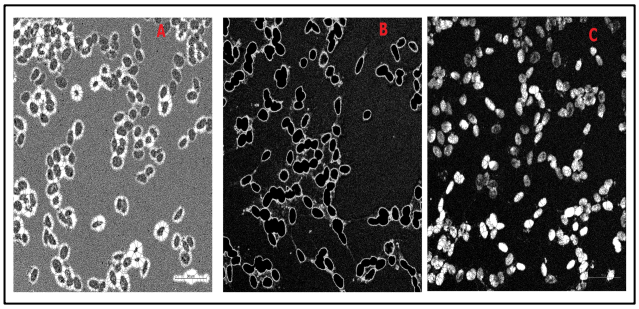

Fig. (26). Microscopic images of MCF-7 cells: (a) control with normal morphology, (b) 5-FU showing apoptotic features, and (c) F1 nanoparticles exhibiting pronounced apoptosis and reduced viability

Mechanistic Considerations

The apoptotic index demonstrated significant induction of programmed cell death by both treatments. Control cells showed minimal apoptosis (4.33 ± 1.00%), confirming culture viability. 5-FU induced robust apoptosis (52.67 ± 6.00%, $p < 0.01$), while F1 nanoparticles achieved 44.00 ± 5.00% ($p < 0.01$ vs. control), representing a 10-fold increase over baseline and comparable to the standard ($p = 0.187$). Microscopy confirmed these findings: control cells upheld normal morphology, while treated cells exhibited cell shrinkage, membrane blebbing, chromatin condensation, detachment, and apoptotic bodies, visually validating the potent cytotoxic effects of both 5-FU and F1.

Significance and Translational Perspective

The results show that F1, a modified chitosan nanoparticle loaded with doxorubicin, is a promising nanomedicine with significant clinical translation potential. In order to ensure optimum, repeatable critical quality attributes (zeta potential, encapsulation, particle size, PDI, efficiency, drug release) appropriate for regulatory compliance, its development adhered to Quality by Design (QbD) principles. The design space was validated by risk assessment (FMEA), experimental design (Box-Behnken), and response surface methods, allowing for scalable manufacturing while upholding stringent quality control. This methodical methodology de-risks the commercialization iof the nanoformulation and facilitates regulatory approval in accordance with FDA and EMA guidelines.[42]

Conclusion

Using a systematic QbD strategy, our study effectively created a doxorubicin-loaded modified chitosan nanoparticle (F1) with optimum physicochemical parameters (size ~223 nm, PDI 0.019, zeta potential −25.3 mV, EE 88%, drug loading 7.52%) and molecular-level drug encapsulation. Through apoptosis (apoptotic index 44%), F1 demonstrated spherical morphology, uniform structure, pH-responsive sustained release, and strong anticancer activity in MCF-7 cells, as demonstrated by MTT, SRB, and XTT experiments. The formulation's tumor-targeted potential was highlighted by its strong intracellular delivery, outstanding biocompatibility, and storage stability. F1 is a therapeutically translatable, cutting-edge nanomedicine platform that combines polymer chemistry, risk-managed formulation design, and thorough characterization, potentially improving therapeutic outcomes in cancer treatment.

Aacknowledgment

The authors sincerely acknowledge the Department of Pharmacy, Dr. Babasaheb Ambedkar Technological University, Lonere, Maharashtra, India, for providing the academic guidance, research facilities, and infrastructure necessary to carry out this Ph.D. research work. The authors are also grateful to the Shivraj College of Pharmacy, Gadhinglaj, Kolhapur, Maharashtra, and the Department of Pharmaceutical Chemistry, Rajrambapu College of Pharmacy, Kasegaon, Maharashtra, India, for their valuable

support, laboratory facilities, and technical assistance during the course of the study.

Conflict of Interest

The authors declare that they have no known competing financial interests or personal relationships that could have appeared to influence the work reported in this paper.

References

1. R. Suresh Kumar, Subhashish Debnath, GNK Ganesh, L Raju, MK Samantha, B Suresh. Chitosan Nano Particles by Ionotropic Gelation Containing L-Arginine. Research J. Pharm. and Tech. 2(1): Jan.-Mar. 2009; Page 80-85.
2. S Rajarajan, R Chandramouli. Preparation, Numerical Optimization and Evaluation of Ciprofloxacin PLGA and PLA Nanoparticles by Solvent Displacement Technique. Research J. Pharm. and Tech. 2(1): Jan.-Mar. 2009; Page 186-190..
3. P Amsa, Abhijit Kosalge, S Tamizharasi, D Karthikeyan, T Sivakumar, Vijay Shinde. Formulation and Evaluation of Chitosan Nanopaticle of Acyclovir. Research J. Pharm. and Tech. 3(1): Jan. - Mar. 2010; Page 121-126.
4. Subhashis Debnath, R. Suresh Kumar, M. Niranjan Babu. Ionotropic Gelation – A Novel Method to Prepare Chitosan Nanoparticles. Research J. Pharm. and Tech. 4(4): April 2011; Page 492-495.
5. Mukesh Kumar D. J., Sonia K., Madhan R., Selvakumar K., Kalaichelvan P.T. Antiyeast, Antioxidant and Anticancer Activity of Tribulus terrestris Linn and Bougainvillea spectabilis Linn. Research J. Pharm. and Tech. 4(9): Sept. 2011; Page 1483-1489.
6. Kalyankar T. M., Butle S. R., Chamwad G. N. Application of Nanotechnology in Cancer Treatment. Research J. Pharm. and Tech. 5(9): September 2012; Page 1161-1167.
7. Prabaharan M. Chitosan derivatives as promising materials for controlled drug delivery. *J Biomater Appl*. 2008; 23(1):5–36.
8. Calvo P, Remuñán-López C, Vila-Jato JL, Alonso MJ. Novel hydrophilic chitosan–polyethylene oxide nanoparticles as protein carriers. *J Appl Polym Sci*. 1997; 63(1):125–132.
9. Bodnar M, Hartmann JF, Borbely J. Preparation and characterization of chitosan-based nanoparticles. *Biomacromolecules***.** 2005; 6(5):2521–2527.
10. Rampino A, Borgogna M, Blasi P, Bellich B, Cesàro A. Chitosan nanoparticles: Preparation, size evolution and stability. *Int J Pharm*. 2013; 455(1–2):219–228.
11. Minotti G, Menna P, Salvatorelli E, Cairo G, Gianni L. Anthracyclines: Molecular advances and pharmacologic developments. *Pharmacol Rev*. 2004; 56(2):185–229.
12. Tacar O, Sriamornsak P, Dass CR. Doxorubicin: An update on anticancer molecular action, toxicity and novel delivery systems. *J Pharm Pharmacol*. 2013; 65(2):157–170.
13. Peer D, Karp JM, Hong S, et al. Nanocarriers as an emerging platform for cancer therapy. *Nat Nanotechnol*. 2007; 2(12):751–760.
14. Gerweck LE, Seetharaman K. Cellular pH gradient in tumor versus normal tissue. *Cancer Res*. 1996; 56(6):1194–1198.
15. Maeda H, Wu J, Sawa T, Matsumura Y, Hori K. Tumor vascular permeability and the EPR effect. *J Control Release***.** 2000; 65(1–2):271–284.
16. ICH Q8 (R2). Pharmaceutical Development. *International Council for Harmonisation*; 2009.
17. Yang TC, Chou CC, Li CF. Antibacterial activity of N-alkylated disaccharide chitosan derivatives. *Int J Food Microbiol.* 2005; 97(3):237–245.ICH Q9. Quality Risk Management. International Council for Harmonisation; 2005.
18. ICH Q10. Pharmaceutical Quality System. *International Council for Harmonisation*; 2008.
19. Montgomery DC. Design and Analysis of Experiments. 8th ed. *Wiley*; 2013.
20. Ferreira SLC, Bruns RE, Ferreira HS, et al. Box–Behnken design: An alternative for optimization. *Anal Chim Acta*. 2007; 597(2):179–186.
21. Rawat M, Singh D, Saraf S, Saraf S. Nanocarriers: Promising vehicle for bioactive drugs. *Biol Pharm Bull*. 2006; 29(9):1790–1798.
22. Higuchi T. Mechanism of sustained-action medication. *J Pharm Sci*. 1963; 52(12):1145–1149.
23. Korsmeyer RW, Gurny R, Doelker E, Buri P, Peppas NA. Mechanisms of solute release from porous hydrophilic polymers. *Int J Pharm*. 1983; 15(1):25–35.
24. Zhang Y, Huo M, Zhou J, Xie S. DDSolver: An add-in program for modeling and comparison of drug dissolution profiles. *The AAPS Journal*. 2010; 12 (3):263–271.
25. Mosmann T. Rapid colorimetric assay for cellular growth and survival: application to proliferation and cytotoxicity assays. *J Immunol Methods.* 1983; 65 (1–2):55–63.
26. Skehan P, Storeng R, Scudiero D, et al. New colorimetric cytotoxicity assay for anticancer-drug screening. *J Natl Cancer Inst.* 1990; 82 (13):1107–1112.
27. Roehm NW, Rodgers GH, Hatfield SM, Glasebrook AL. An improved colorimetric assay for cell proliferation and viability utilizing the tetrazolium salt XTT. *J Immunol Methods.* 1991; 142 (2):257–265.

28. Strober W. Trypan blue exclusion test of cell viability. *Curr Protoc Immunol.* 2001; 21: A3.B.1–A3.B.2.
29. Freshney RI. Culture of animal cells: a manual of basic technique and specialized applications. 6th ed. Hoboken (NJ): *Wiley-Blackwell;* 2010.
30. Aditee Mishal, Sudha Rathod. Quality by Design: A New Era of Development of Quality in Pharmaceuticals. Research J. Pharm. and Tech. 7(5): May, 2014; Page 581-591.
31. Hancock BC, Zografi G. Characteristics and significance of the amorphous state. *J Pharm Sci***.** 1997; 86 (1):1–12.
32. Mosmann T. Rapid colorimetric assay for cellular growth and survival (MTT). *J Immunol Methods***.** 1983; 65 (1–2):55–63.
33. Skehan P, Storeng R, Scudiero D, et al. New colorimetric cytotoxicity assay (SRB). *J Natl Cancer Inst***.** 1990; 82 (13):1107–1112.
34. Roehm NW, Rodgers GH, Hatfield SM, Glasebrook AL. An improved colorimetric assay (XTT). J Immunol Methods. 1991; 142 (2):257–265.
35. Elmore S. Apoptosis: A review of programmed cell death. *Toxicol Pathol***.** 2007; 35 (4):495–516.
36. Florence AT, Hussain N. Transcytosis of nanoparticle and drug delivery. *Adv Drug Deliv Rev*. 2001;50 (Suppl 1):S69–S89.
37. Blanco E, Shen H, Ferrari M. Principles of nanoparticle design for cancer therapy. *Nat Biotechnol.* 2015; 33 (9):941–951.
38. FDA. Considering whether an FDA-regulated product involves nanotechnology. Guidance for Industry. 2014.
39. EMA. Reflection paper on nanotechnology-based medicinal products. EMA; 2011.
40. Siepmann J, Siepmann F. Mathematical modeling of drug delivery**.** *Int J Pharm***.** 2008; 364 (2):328–343.
41. Costa P, Sousa Lobo JM. Modeling and comparison of dissolution profiles. *Eur J Pharm Sci***.** 2001; 13 (2):123–133.